Available online at www.sciencedirect.com
ScienceDirect
Catalysis Today 127 (2007) 165–175
CATALYSIS TODAY
www.elsevier.com/locate/cattod

On the quantitative aspects of hydrolysis of isocyanic acid on TiO_2

Philipp Hauck, Andreas Jentys, Johannes A. Lercher *

Department of Chemistry, Institute for Chemical Technology, Technische Universität München, Lichtenbergstrasse 4, D-85747 Garching, Germany

Available online 3 July 2007

Abstract

The selective catalytic reduction with aqueous solutions of urea is currently seen having the highest potential to reduce NO_x and particulate emissions for commercial diesel powered vehicles. Ammonia as the actual reduction medium is formed from urea in two consecutive reactions, i.e. via the thermolysis of urea to isocyanic acid and NH_3 and the catalyzed hydrolysis of HNCO over TiO_2 to NH_3 and CO_2. A kinetic model for the hydrolysis reaction was derived for a reaction scheme comprising a set of elementary steps. To minimize the number of unknown variables in the kinetic model for the overall rate, the equilibrium constants for both reactants (HNCO and H_2O) and products (NH_3 and CO_2) were determined from adsorption isotherms using Langmuir and multilayer adsorption models. A data set consisting of 49 data points for the rate determined at varying reactant concentrations was fitted with the kinetic model using a non-linear least mean squares regression analysis.

Keywords: Diesel emission; SCR; DeNO$_x$; Urea; Hydrolysis; Isocyanic acid; Adsorption; TiO_2; Anatase; Kinetic model; Rate

1. Introduction

Approximately 20% of the current global anthropogenic nitrogen oxide emissions originate from passenger cars and commercial vehicles [1], and it is foreseen that the increasingly rigid emission standards for NO_x being introduced by European and US legislation over the next years can only be fulfilled by exhaust gas after-treatment technology. Today, the selective catalytic reduction (SCR) with ammonia is considered as the most promising technique for reducing NO_x emissions from heavy-duty diesel engines [2–5]. However, the use of gaseous NH_3 requires elaborate safety precautions for handling and storage. Therefore, the European Automobile Manufacturers Association decided to recommend urea for the on-board production of the reducing agent NH_3 [6]. At present in most applications an aqueous urea solution (AdBlue®, i.e. a solution of 32.5% urea in H_2O) is injected into the exhaust gas stream.

Resulting from the typical spatial constraints of cars, the catalyst volume is aimed to be minimal. However, this is met with difficulties, as the dynamically varying loads of the engine drastically affect the reaction conditions for the catalyst [7]. To avoid overdosing and consequently the release of NH_3 under dynamic conditions a complex strategy is required. Several engineering design variants have been proposed suggesting urea decomposition reactors that are incorporated into the exhaust system or are built as separate units [8,9]. The most effective design introduced so far is an external monolithic hydrolysis catalyst heated by a partial stream of the exhaust gas. For a further optimization of the hydrolysis process a detailed knowledge of the kinetics of the (thermal and catalytic) transformation of urea into ammonia is essential [8].

The conversion of the aqueous urea solution to ammonia consists of two steps. In the first step, the aqueous urea solution is sprayed into the flue gas stream. After evaporation of H_2O, the remaining urea decomposes thermally into ammonia and isocyanic acid according to (1).

$$H_2N{-}CO{-}NH_2(s) \rightarrow NH_3(g) + HNCO(g) \quad (1)$$

In the second step, the isocyanic acid is hydrolyzed over an oxide catalyst yielding ammonia and carbon dioxide according to (2).

$$HNCO(g) + H_2O(g) \rightarrow NH_3(g) + CO_2(g) \quad (2)$$

It should be noted, however, that isocyanic acid can also undergo a series of condensation reactions leading to solid products ranging from cyanuric acid and biuret over ammelide and ammeline and melamine to polymeric forms of melamine [3,8,10]. These high molecular weight compounds have been

* Corresponding author. Tel.: +49 89 28913540; fax: +49 89 28913544.
E-mail address: johannes.lercher@ch.tum.de (J.A. Lercher).

0920-5861/$ – see front matter © 2007 Elsevier B.V. All rights reserved.
doi:10.1016/j.cattod.2007.05.012

reported [3] to deposit on the walls of the exhaust pipe and inside the monolith channels and are only slowly decomposed under the typical reaction conditions, which leads to severe catalyst deactivation. In order to minimize the formation of these polymeric species, the reaction conditions and the catalysts have to be optimized to maximize the rate of hydrolysis and to minimize condensation/oligomerization reactions of isocyanic acid.

The present work introduces a kinetic model for the overall rate of the HNCO hydrolysis on TiO_2 anatase, which is the well-established catalyst for hydrolysis reactions. Values for the adsorption equilibrium constants of the reactants HNCO and water as well as of the products ammonia and carbon dioxide were determined experimentally from sorption isotherms (by IR spectroscopy and gravimetry) and implemented into the kinetic model. Thus, the sensitivity of the model was enhanced by reducing the number of unknown variables being determined.

2. Experimental

2.1. Catalyst

The hydrolysis catalyst was TiO_2 in anatase form obtained from Süd-Chemie AG and coated onto a metal substrate obtained from Emitec. Textural promoters and/or binders (inorganic sol) were added to enhance the mechanical stability of the coating and to increase the adhesive strength to the metal foil, respectively. This catalyst is a typical formulation used in heavy-duty diesel trucks in the technical application. For studying the sorption of reactants and products by IR spectroscopy TiO_2 from the same source was used in powder form. TiO_2 was synthesized following the sulfate process in which titanium slag obtained by reduction of ilmenite $FeTiO_3$ with coke at around 1200 °C is treated with concentrated sulfuric acid at 100–180 °C [11]. The preparation process of TiO_2 is the origin of sulfate impurities observed by IR spectroscopy, which are discussed in the paper.

The specific surface area of the TiO_2 determined by the BET method was 80 m^2/g.

2.2. Preparation of isocyanic acid

The synthesis of isocyanic acid was carried out by the depolymerization of commercial cyanuric acid catalyzed by Al_2O_3 according to the method developed by Lercher and Zhan [12]. A heated quartz tubular reactor (18 mm i.d.) separated into three sections was used. The first section of the reactor was filled with quartz spheres to preheat the He carrier gas stream. The second section of the reactor contained 15 g of cyanuric acid (sublimation temperature 593–603 K), and the third section of the reactor held the Al_2O_3 catalyst used to depolymerize cyanuric acid. By using a catalyst, the decomposition temperature of the cyanuric acid could be lowered to $T = 643$ K compared to 753 K for thermal decomposition, which leads to a high purity of the product (less than 1 vol.% NH_3 and less than 1000 ppm CO_2). Downstream of the reactor, the gaseous HNCO was condensed in two serial cold traps at 193 K (isopropanol/dry ice). To obtain a CO_2 and NH_3 free product it is essential to bypass the cold traps during start-up of the reaction [13]. The depolymerization has to be performed in the absence of water, as Al_2O_3 not only catalyzes the depolymerization but also the hydrolysis of HNCO.

2.3. In situ infrared spectroscopy

Infrared spectra were measured with a Bruker IFS 88 FTIR spectrometer in a vacuum cell that allows to collect IR spectra *in situ* during activation and adsorption [14]. The spectra were recorded with a resolution of 4 cm^{-1} using a MCT detector. The catalyst samples were pressed into thin, self-supporting wafers (~5 mg cm^{-2}) and placed in a heatable sample-holder in the center of the IR cell equipped with CaF_2 windows. The samples were heated in vacuum ($p < 10^{-6}$ mbar) to 673 K (10 K min^{-1} increment). After reaching the activation temperature, O_2 with 1 mbar equilibrium pressure was introduced into the cell for 60 min in order to saturate the oxygen vacancies on the surface. The samples were subsequently cooled to 393 K in the O_2 atmosphere and evacuated. With this procedure the white color of the titania sample could be restored indicating the saturation of defect sites of TiO_2.

Ammonia, water, isocyanic acid and carbon dioxide were adsorbed at 393 K at equilibrium pressures between 10^{-4} and 10^{-1} mbar. For isocyanic acid the desorption was investigated by heating the sample from 393 to 673 K in vacuum (10 K min^{-1} increment). The surface coverage of the adsorbate was determined form the integral intensity of the characteristic IR bands.

2.4. Thermogravimetry

The sorption isotherm for water was additionally measured on a Setaram TG–DSC 111 thermoanalyzer. The sample (~20 mg) was activated at 673 K for 1 h (heating rate 10 K min^{-1}) under vacuum ($p < 10^{-7}$ mbar). Water was adsorbed at 393 K using stepwise pressure increments from 3×10^{-3} up to 16.1 mbar, and the weight increase was measured.

2.5. Kinetic measurements

The experimental set-up used for the kinetic experiments is shown in Fig. 1. The composition of the feed gas was chosen to present a typical diesel exhaust gas, containing 4% H_2O and 10% O_2 with N_2 being the balancing gas [5,15]. The gas flow rates were controlled using electronic mass flow controllers, and water was dosed through a fused silica capillary (0.1 mm i.d.) into the electrically heated heating block by means of a HPLC pump. HNCO was introduced into the system via an additional N_2 stream and a saturator, which was maintained at −30 °C; the standard concentration of HNCO was 500 ppm.

For the kinetic experiments aiming at the individual order of reaction, the concentration of the corresponding reactant or product, respectively, was varied over a reasonable range, and the rate was calculated.

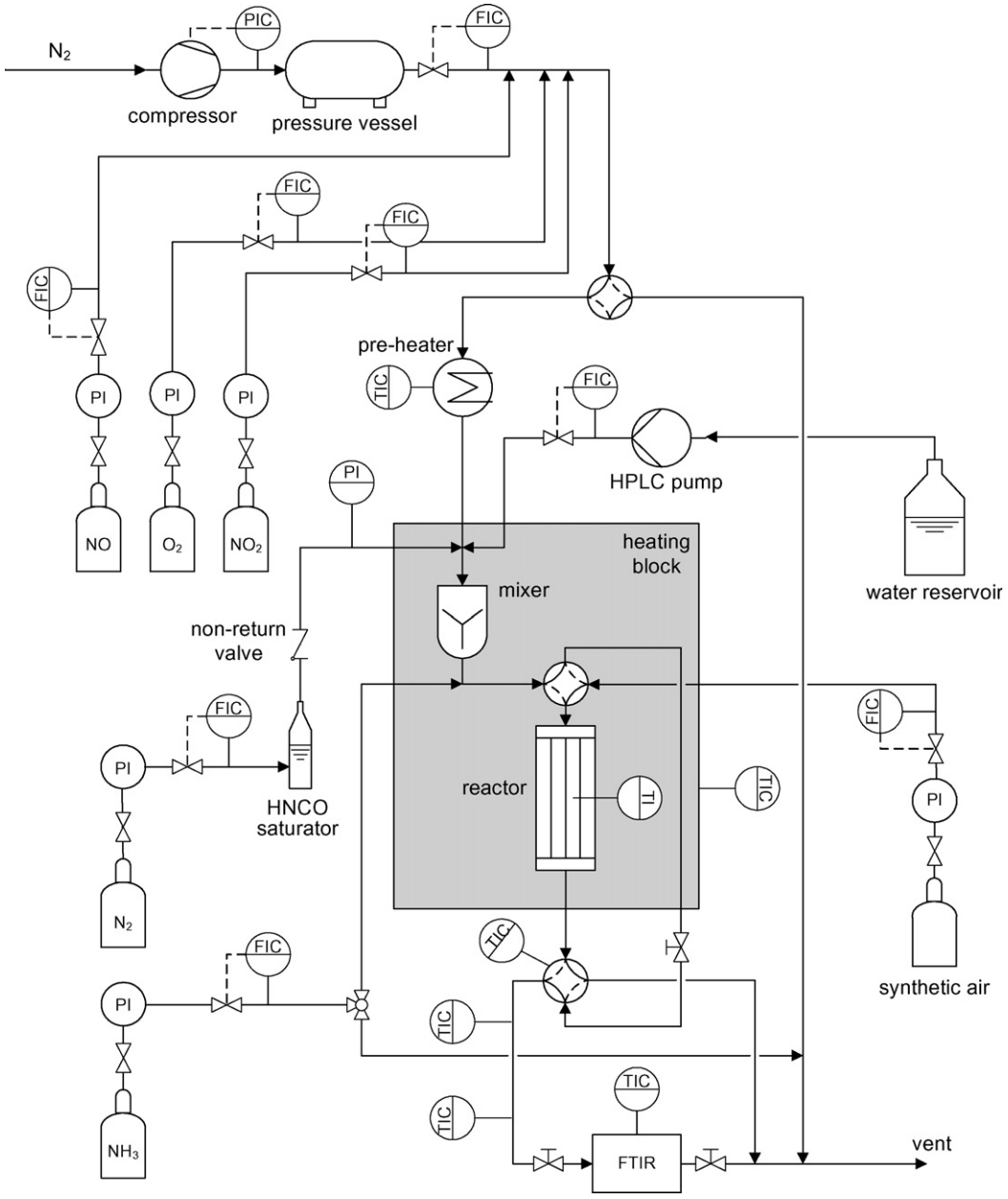

Fig. 1. Flow scheme of the reaction system.

The rate of the HNCO hydrolysis was determined using the active material coated onto a metal sheet to resemble the material in the technical application. The reactor was built from stainless steel with a rectangular cross section of dimensions 3.5 mm × 2 mm (width × height) (Fig. 2). The catalyst was tested as a single coated metal sheet of 10 mm length and a thickness of 110 μm, simulating a two channel monolithic structure with a cell density of 185 cpsi. The mass of active material exposed to the gas stream was 1.75 mg (calculated from the layer thickness and the packing density of the TiO_2 coating). The total flow rate was typically 3.6 l_N/min, and the geometric surface area of the catalyst was 70 mm^2. A thermocouple was incorporated in the reactor block for a direct measurement of the catalyst temperature. As the catalytic material employed was highly active, these very short residence

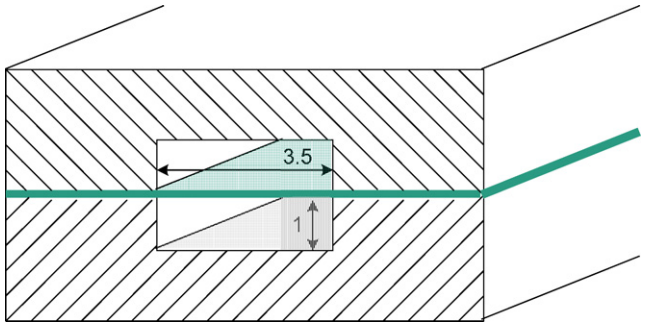

Fig. 2. Design of flat bed reactor with internal simulating a two channel monolithic structure.

times (areal velocity AV = volumetric flow rate/catalyst geometric surface area ≈3100 m_N/h) were necessary to reach differential reaction conditions (equivalent to conversion $X_{HNCO} \leq 10\%$).

The gas composition was continuously analyzed by a FTIR spectrometer (Thermo Electron Corporation Nexus, OMNIC QuantPad software) equipped with a heated, low volume multiple-path gas cell (2 m). The tubes connecting the reactor outlet and the gas cell in the IR spectrometer as well as the gas cell itself were heated to 185 °C in order to prevent condensation/polymerization of HNCO at cold spots. The quantification method developed allowed to monitor concentrations in the ppm range of 25 compounds in total, including HNCO. Results were independent of the batch of synthesized HNCO and the mass balances based on carbon and nitrogen were better than 99%.

3. Results and discussion

3.1. Adsorption isotherms derived from IR spectroscopy

The IR spectra of the activated sample and after adsorption of NH_3 at partial pressures of 1×10^{-3}, 1×10^{-2} and 1×10^{-1} mbar are shown in Fig. 3. Sorption of NH_3 led to a decrease of the intensity of the bands assigned to the hydroxyl groups of TiO_2 (3714 and 3666 cm^{-1}) [16,17] and to the simultaneous formation of bands at 3388, 3352, 3260, 3199 and 3160 cm^{-1}. The observed multiplet in the NH stretching region can be assigned to the asymmetric and symmetric stretching vibrations (ν_{NH}) as well as to the first overtone of the asymmetric deformation band of two chemisorbed NH_3 species [18]. An evidence for the presence of two types of Lewis sites for the sorption of NH_3 on the surface of anatase is the splitting of the symmetric deformation band (1211 and 1169 cm^{-1}) [19,20]. The asymmetric deformation band at 1605 cm^{-1} is known to be less sensitive to the strength of the coordination band and thus appears unsplit. The band at 1371 cm^{-1}, present in the activated sample (spectrum (a) in Fig. 3) is attributed to the characteristic $\nu_{S=O}$ vibration of sulfate species [21,22], which resulted from impurities during the synthesis of the particular TiO_2 sample. Upon adsorption of NH_3 two new bands were observed at 1338 and 1314 cm^{-1} while the band at 1371 cm^{-1} disappeared, which indicates the breaking of the Ti–O–S bonds upon the interaction of NH_3 with the sulfate groups and the formation of Ti–NH_2 species (similar to the adsorption of water described in the following paragraph).

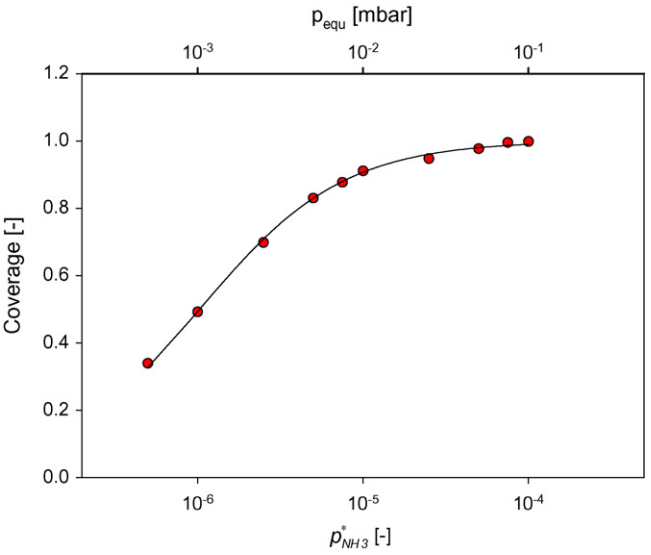

Fig. 4. Adsorption isotherm of NH_3 on TiO_2 anatase, T_{Ads} = 393 K.

The surface coverage was calculated from the intensity of the symmetric deformation band of NH_3 at 1605 cm^{-1}, and the sorption isotherm was described with the Langmuir model (Fig. 4):

$$\Theta_i = \frac{K_i p_i^*}{1 + K_i p_i^*} \quad (3)$$

in which $K_i = k_{i,ads}/k_{i,des}$ is the equilibrium constant and p_i^* is the pressure normalized to standard conditions ($p^* = p/p_0$ with p_0 = 1013.25 mbar). From the fit of the experimental data to a Langmuir isotherm $K_{NH_3} = 9.73 \times 10^5$ was determined.

The IR spectra during H_2O adsorption at pressure between 3×10^{-4} and 6×10^{-1} mbar are shown in Fig. 5. In presence of

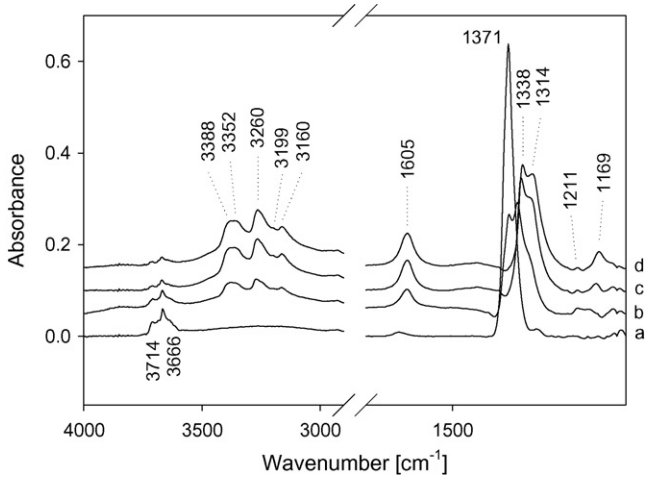

Fig. 3. IR spectra during NH_3 adsorption on TiO_2 anatase, T_{Ads} = 393 K. (a) Activated sample, (b) 1×10^{-3}, (c) 1×10^{-2} and (d) 1×10^{-1} mbar NH_3.

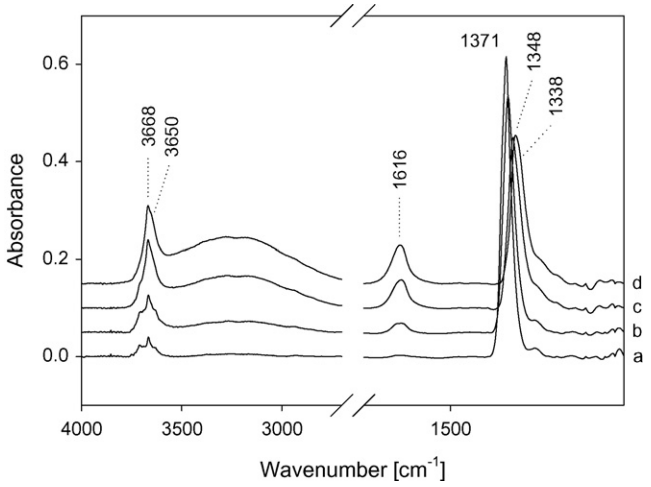

Fig. 5. IR spectra during H_2O adsorption on TiO_2 anatase, T_{Ads} = 393 K. (a) Activated sample, (b) 1×10^{-3}, (c) 1×10^{-2} and (d) 1×10^{-1} mbar H_2O.

water, the intensity of the hydroxyl bands (3668 and 3650 cm^{-1}) strongly increased, accompanied with the appearance of a broad band between 3500 and 3000 cm^{-1}. According to Knözinger [23], water molecules adsorb dissociatively on five-coordinate Ti^{4+} cations with the O^{2-} ions bridging two cations and form two types of surface OH groups—a monodentate terminal and another bidentate bridged hydroxyl. The band at 1616 cm^{-1} can be clearly assigned to the deformation vibrations of water molecules [24]. The band of the sulfate groups at 1371 cm^{-1} decreased in intensity and shifted gradually to 1348 cm^{-1}, which indicates a strong interaction with the water molecules adsorbed. Simultaneously a new band was observed at 1338 cm^{-1} as a shoulder in spectrum (d) in Fig. 5. At the highest H_2O concentration applied ($p_{equ} = 6 \times 10^{-1}$ mbar) the latter band was predominant, while the band at 1348 cm^{-1} has disappeared. Saur et al. [22] studied this effect and postulated a change from structure II into III:

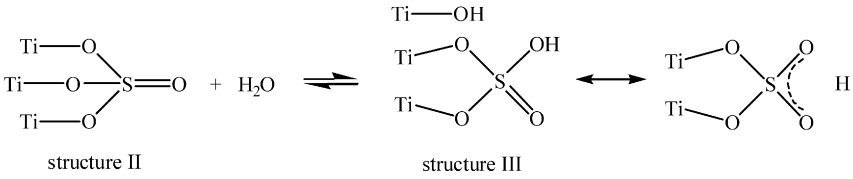

The sorption isotherm of H_2O was determined from the intensity of the band at 1616 cm^{-1} and described with the BET isotherm Type II [25], which is the most commonly used isotherm for multilayer adsorption:

$$\frac{V}{V_{Mono}} = \frac{cz}{(1-z)[1-(1-c)z]} \quad \text{with} \quad z = \frac{p}{p'}. \tag{4}$$

In this expression p' denotes the vapor pressure above an adsorbate layer of more than one molecule thickness (similar to a normal liquid), which is 1.81 bar at 393 K [26]. V_{Mono} is the adsorbed gas volume corresponding to the monolayer and c is a constant that can be considered as an equilibrium constant for the first layer.

Eq. (4) can be written as

$$\frac{z}{(1-z)V} = \frac{1}{cV_{Mono}} + \frac{(c-1)z}{cV_{Mono}}. \tag{5}$$

When plotting the left hand side of Eq. (5) versus z (see Fig. 6), V_{Mono} and c can be calculated from the slope and ordinate intercept of the resulting straight line. Thus, $V_{Mono} = 5.432$ and $c = 1.24 \times 10^5$ were obtained. Note that the value retrieved here for V_{Mono} has arbitrary units as the underlying quantitative measure was peak area.

During adsorption of HNCO on the TiO_2 sample at 393 K the intensity of the surface species suddenly increased, when the equilibrium pressure was raised from 6×10^{-3} to 1×10^{-2} mbar (see Fig. 7(B)). Most of the IR bands observed are already discussed in detail in the literature—a few still with controversy. The most intense band at 2206 cm^{-1} starts to evolve at 3×10^{-3} mbar and shifts gradually to 2230 cm^{-1} with increasing partial pressure. Two shoulders at 2189 and 2255 cm^{-1} were observed, developing at an equilibrium pressure of 1×10^{-2} and 3×10^{-2} mbar, respectively. In agreement with literature (e.g. Fischer et al. [27,28]), we assign the band in the range 2206–2230 cm^{-1} to the asymmetric stretching vibration of isocyanate species –NCO. HNCO adsorbs dissociatively on metal oxides forming isocyanates bound to Lewis acid sites [29]. The counter ions proposed are five-coordinate Ti^{4+} ions (O^{2-} ions bridging two cations) in the (0 0 1) plane of anatase [23]. Zhan [13] also observed two shoulders during adsorption of HNCO on Al_2O_3 and assigned the one at higher wavenumber (at 2281 cm^{-1}, the main peak being at 2257 cm^{-1}) to weakly adsorbed HNCO due to its possible removal at mild conditions and the one at lower wavenumber (2238 cm^{-1}) to cyanamide species N–C≡N formed through the reaction of isocyanic acid with traces of ammonia. Another indication of the dissociative adsorption of HNCO is the appearance of two bands at 3511 and 3452 cm^{-1} (see Fig. 7(A)), which can be both assigned to perturbed OH groups resulting from the (hydrogen bonding) interaction with surface NCO^- groups [17,27]. Three further bands (3377, 3259 and 3154 cm^{-1}) result from NH stretching modes.

The bands at 1645, 1560 and 1500 cm^{-1} with additional smaller bands in the region 1750–1400 cm^{-1} deserve special attention. Piazzesi et al. [30], who adsorbed HNCO on anatase at 423 K, tentatively attributed these bands to cyanuric acid formed by a polymerization of HNCO and/or to s-triazine formed by a reaction of HNCO with traces of NH_3 adsorbed on the surface. In contrast Acke et al. [31] exposed γ-Al_2O_3 to

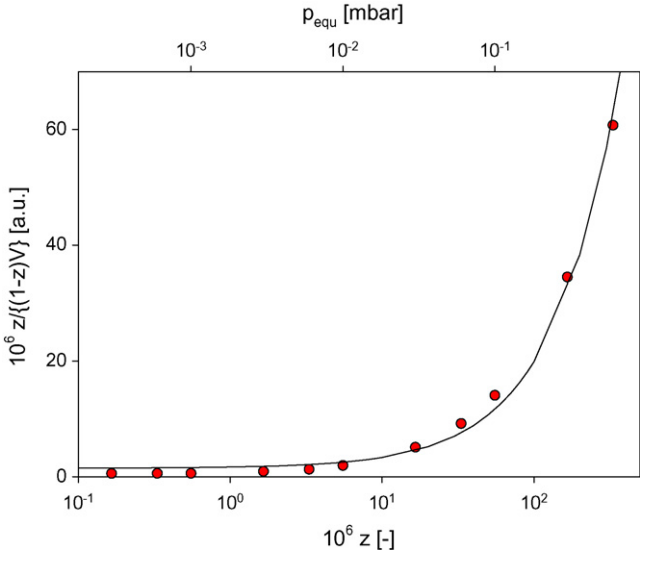

Fig. 6. BET adsorption isotherm of H_2O on TiO_2 anatase, $T_{Ads} = 393$ K.

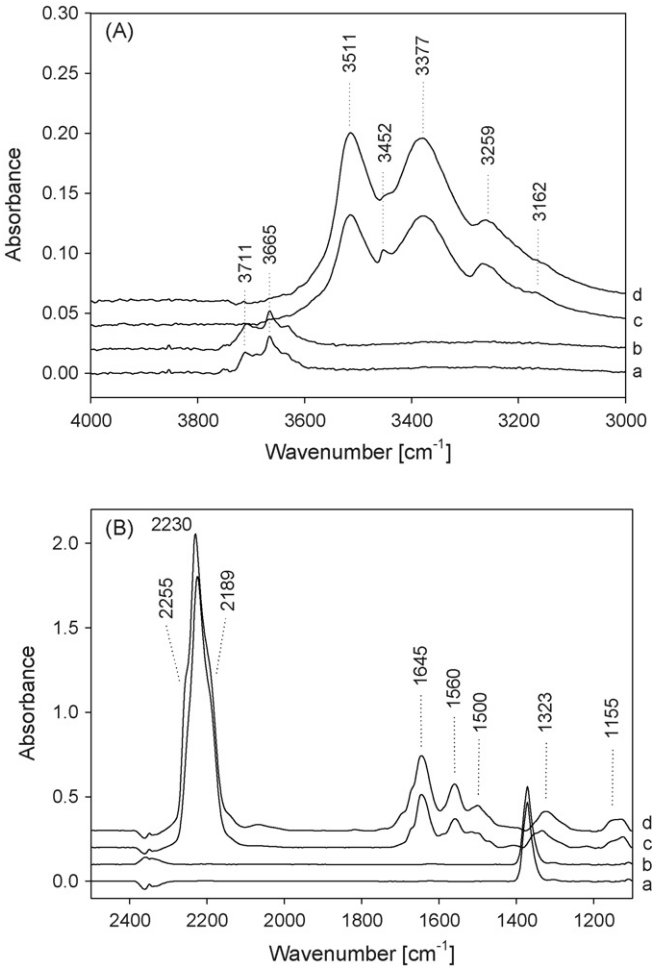

Fig. 7. (A and B) IR spectra of HNCO adsorption on TiO_2 anatase, T_{Ads} = 393 K. (a) Activated sample, after adsorption of (b) 1×10^{-3}, (c) 1×10^{-2} and (d) 1×10^{-1} mbar HNCO.

HNCO and O_2 and assigned the bands at 1656, 1587 and 1500 cm^{-1} to surface coordinated ammonia and ammonium ions. Larrubia et al. [32] found bands at 1650, 1565 and 1490 cm^{-1} after adsorption of urea on Fe_2O_3-TiO_2 and V_2O_5-MoO_3-TiO_2 SCR catalysts and acetamide over Al_2O_3 and Fe_2O_3, respectively, and assigned them to an anionic adsorbed species of the corresponding molecules. On the basis of these experiments we propose that the bands at 1645, 1560 and 1500 cm^{-1} are not due to only one intermediate species, but rather result from different species co-existing on the surface after HNCO adsorption following earlier work in our group [13]. In addition own LDA calculations of the vibrational frequencies of urea and acetamide indicate three characteristic vibrations in the region 1810–1429 cm^{-1} which are C=O stretching, NH_2 deformation and asymmetric C–N stretching modes (in the case of acetamide additional CH_3 ''umbrella'' deformation vibration) in descending wavenumber sequence. The observed band at 1645 cm^{-1} is therefore tentatively assigned to the carbonyl stretching vibration of either Ti–NCO and/or trimer-adsorbed HNCO–cyanuric acid, whereas the band at 1560 cm^{-1} (NH_2 deformation) can be assigned to either melamine or Ti–N=C(OH)(NH_2) which is formed by reaction of carbodiimide Ti–N=C=N–H with water. The band at 1500 cm^{-1} is tentatively assigned to asymmetric C–N stretching modes of cyanuric acid, melamine and/or adsorbed cyanamide Ti–NH–C≡N, the latter one being the isomer of carbodiimide and formed through reaction of HNCO with traces of NH_3 on the catalyst surface [13]. The sulfate groups (band at 1371 cm^{-1}) strongly interact with HNCO, which led to the disappearance of the band after increasing the equilibrium pressure from 6×10^{-3} to 1×10^{-2} mbar. Note that at the same time the intensity of the isocyanate band at 2206 cm^{-1} increased simultaneously. Two broad bands with low intensity at 1323 and 1155 cm^{-1} can be observed in spectra (c and d) in Fig. 7(B). We tentatively assign the latter one to traces of NH_3 which is formed by hydrolysis of HNCO on the surface OH groups of titania.

In order to further investigate the surface species of HNCO on TiO_2, the desorption was followed by *in situ* IR spectroscopy. After evacuation at 673 K, the band at 2230 cm^{-1}, attributed to isocyanate species, strongly decreased in intensity, and the bands in the region 1750–1400 cm^{-1} disappeared completely. In parallel, the intensity of the sulfate band at 1371 cm^{-1} was restored (Fig. 8). This demonstrates the partially reversible character of the sorption/reaction processes. Solid cyanuric acid decomposes between 593 and 603 K [10], and the isocyanic acid released is not strongly adsorbed at 673 K. Simultaneously new bands were observed at 2030 and 2014 cm^{-1}. The band at 2072 cm^{-1}, which was already present during HNCO adsorption, increased in intensity. It is tentatively ascribed to carbodiimide species –N=C=NH formed in combination with carbon dioxide via disproportionation of isocyanic acid [12,33]. After evacuation in presence of 1 mbar O_2 at 673 K, almost all polymeric HNCO surface species were removed, except for one species represented by the band at 2030 cm^{-1} (see spectrum (c) in Fig. 8).

To obtain the thermodynamic equilibrium constant for the HNCO adsorption, the intensity of the characteristic band in the range 2206–2230 cm^{-1} was used. It should be noted that this

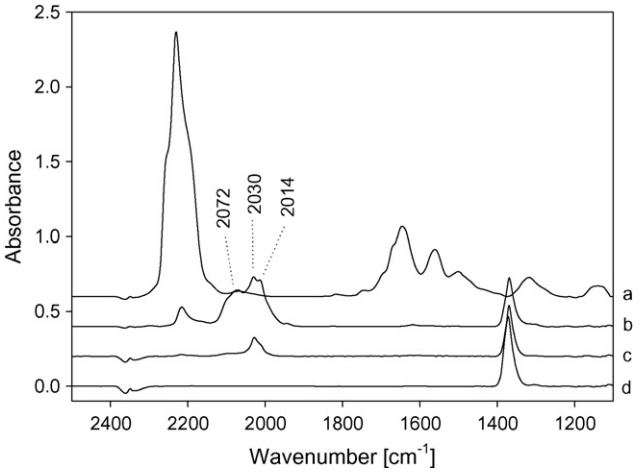

Fig. 8. IR spectra of HNCO adsorption (3×10^{-1} mbar) on TiO_2 anatase, T_{Ads} = 393 K (a), followed by evacuation at 673 K (b) and after exposure to 1 mbar of O_2 at 673 K (c). For comparison activated sample before adsorption experiment (d).

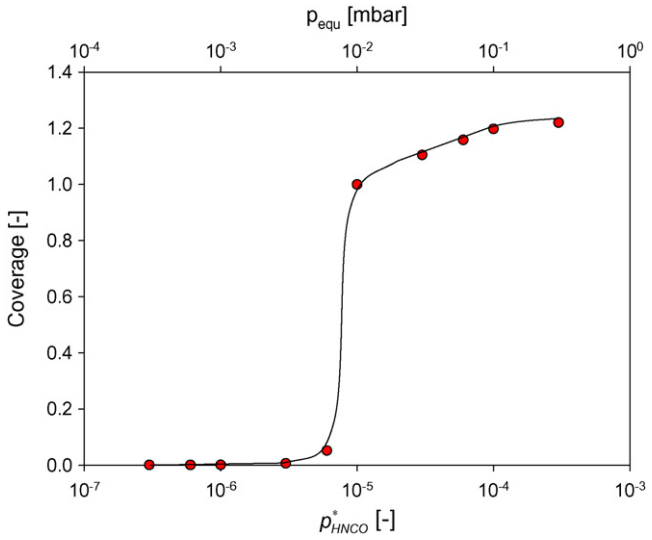

Fig. 9. Adsorption isotherm of HNCO on TiO_2 anatase, T_{Ads} = 393 K.

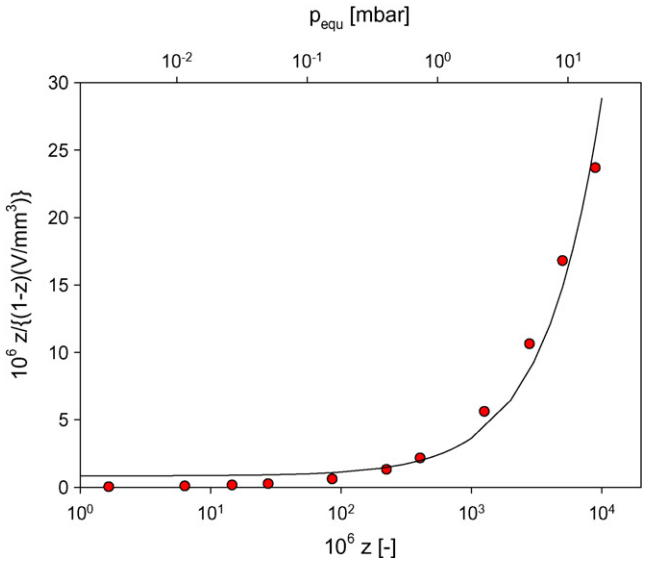

Fig. 10. BET adsorption isotherm of H_2O on TiO_2 anatase from thermogravimetry, T_{Ads} = 393 K.

region includes isocyanate and possibly traces of cyanamide species. A peak deconvolution, however, was not performed as the cyanamide contribution to the peak area was below 5%. The sorption isotherm of HNCO over TiO_2 given in Fig. 9 shows a sudden increase in the surface coverage of HNCO at an equilibrium pressure of 1×10^{-2} mbar. At this equilibrium pressure all OH groups (3711, 3665 cm^{-1}) were covered, thus we defined this point as complete coverage. The IR spectra (Fig. 7(B)) indicated that HNCO undergoes a chemical reaction (most likely trimerization to cyanuric acid) on the titania surface in addition to the dissociative adsorption. For this reason the equilibrium constant could not be extracted from this experiment.

During adsorption of CO_2 on TiO_2 at 393 K in the pressure range from 5×10^{-4} to 1 mbar a significant surface concentration of adsorbed carbonates, which are typically observed at 1580 and 1320 cm^{-1} [23] was not detected. This is consistent with the kinetic experiments, which revealed a zero order dependence of the reaction rate of HNCO hydrolysis with respect to CO_2. This means that under the investigated conditions carbon dioxide does not interact noticeably with the titania surface, but shows inert behavior, and thus no effect in the kinetics is seen on variation of the CO_2 concentration.

3.2. H_2O adsorption isotherm by thermogravimetry

The monolayer sorption capacity for H_2O was additionally determined by thermogravimetry. Similar to the IR data, the BET isotherm expressed in Eq. (4) was used to model the sorption isotherm. It should be noted at this point that the maximum partial pressure of H_2O achievable within the constraints of the experimental set-up was 16 mbar, which is of the same order of magnitude as the water content of a typical diesel exhaust gas (4–5% according to ref. [34]).

V_{Mono} = 357 mm^3 (corresponds to m_{cat} = 21.31 mg) and c = 3306 were determined from the BET plot shown in Fig. 10. Thus, the area-related surface concentration of H_2O when the monolayer is predominant is calculated as $\hat{c}_{Mono} = 9.31 \times 10^{-6}\,mol/m^2$. The area-related surface concentration can be translated into the more suitable units [mol/l] regarding the rate of reaction by means of the following equation

$$c_{Mono} = (1 - \varepsilon)\rho_a\,BET\,\hat{c}_{Mono}, \quad (6)$$

in which ε denotes the porosity of the catalyst bed (estimated to be 0.5) and ρ_a the apparent density of the catalyst, which is estimated to be half of the real density (ρ_a = 1.94 g/cm^3). Thus, c_{Mono} = 0.722 mol/l is obtained, which can be applied in the kinetic model.

3.3. Rate expression

The overall reaction scheme compiled in Table 1 is proposed for the hydrolysis of isocyanic acid over TiO_2 anatase based on

Table 1
Reaction scheme proposed for the Langmuir-Hinshelwood mechanistic model

Reaction, rate equation
(1) Dissociative adsorption of isocyanic acid to yield surface isocyanates
$HNCO + Ti^{4+} + Ti{-}OH \rightleftarrows Ti{-}NCO + Ti{-}OH_2$
$r_1 = k_1\,p_{HNCO}[Ti^{4+}][Ti{-}OH] - k_{-1}[Ti{-}NCO][Ti{-}OH_2]$
(2) Molecular adsorption of water
$H_2O + Ti^{4+} \rightleftarrows Ti{-}OH_2$
$r_2 = k_2\,p_{H_2O}[Ti^{4+}] - k_{-2}[Ti{-}OH_2]$
(3) Surface reaction according to Langmuir–Hinshelwood mechanism
$Ti{-}NCO + Ti{-}OH_2 \rightleftarrows Ti{-}NH_2 + Ti^{4+} + CO_2$
$r_{s1} = k_{s1}[Ti{-}NCO][Ti{-}OH_2]$ (only forward reaction)
(4) Formation of ammonia
$Ti{-}NH_2 + Ti{-}OH_2 \rightleftarrows Ti{-}NH_3 + Ti{-}OH$
$r_{s2} = k_{s2}[Ti{-}NH_2][Ti{-}OH_2] - k_{-s2}[Ti{-}NH_3][Ti{-}OH]$
(5) Desorption of ammonia and regeneration of active site
$Ti{-}NH_3 \rightleftarrows NH_3 + Ti^{4+}$
$r_3 = k_3\,p_{NH_3}[Ti^{4+}] - k_{-3}[Ti{-}NH_3]$

in situ IR studies reported previously [27]. In presence of 4 vol.% H_2O the main surface species observed during hydrolysis reaction were (i) molecularly adsorbed water, (ii) isocyanate (Ti–NCO) species bound to accessible Ti^{4+} cations and (iii) NH_3. Note that the same surface species were observed in additional studies on a sulfate free TiO_2 anatase catalyst, which was synthesized in-house by the hydrolysis of titanium tetraisopropanolate $Ti[OCH(CH_3)_2]_4$ [35].

On the TiO_2 anatase surface, polar hydroxyl groups Ti–OH are present as well as (coordinate) unsaturated Ti^{4+} and Ti^{3+} ions, which are strong Lewis acidic electron-pair-acceptor sites [17,24,36]. In the proposed reaction scheme Ti–OH_2 denotes molecularly (non-dissociative) adsorbed water on Ti^{4+} cations. We assume two different active sites for H_2O molecule adsorption, i.e. Ti^{4+} ions having one or two coordinative unsaturations with respect to the octahedral overall coordination sphere of Ti^{4+} cations in the bulk.

Applying the concept of the rate determining step to the postulated reaction scheme, we start by assuming that the rate limiting elementary step is part of the convoluted surface reaction (Reaction (3) in Table 1), while all other reactions are quasi equilibrated, i.e. those rates are significantly faster and therefore the rate of the forward and backward reaction is the same. The resulting expression for the overall rate of reaction is therefore

$$r = k_s[\mathrm{Ti{-}NCO}][\mathrm{Ti{-}OH_2}] \tag{7}$$

in which [Ti–NCO] and [Ti–OH_2] denote the reactant concentrations on the catalyst surface. The backward reaction is omitted, as a calculation of the thermodynamic equilibrium showed that the products are favored by eight orders of magnitude in the temperature range 393–773 K.

The kinetic data were collected over the TiO_2 anatase catalyst at $T = 393$ K under differential reaction conditions using the experimental set-up described in ref. [27]. The low temperature was chosen in order to stay in the kinetically controlled regime, while at higher temperatures mass transfer processes additionally contribute to the reaction rate. In the temperature regime between 383 and 403 K the apparent activation energy of 73 kJ/mol was observed [27]. The concentrations of the reactants and products were varied systematically (see Table 2) to obtain a reliable set of data for the fitting of the kinetic parameters. The complete data set consists of 49 data points.

Table 2
Description of data sets used for fitting of rate expression

Data set #	$[HNCO]_0$ in ppm	$[H_2O]_0$ in vol.%	$[NH_3]_0$ in ppm	Number data points
1	52 – 999	4[a]	0[a]	11
2	500[a]	0.2 – 10	0[a]	10
3	500[a]	4[a]	0 – 1311	8
4	97 – 1461	4[a]	0[a]	7
5	61 – 900	0.3 – 10	0[a]	7
6	500[a]	4[a]	61 – 1324	6

[a]Standard reaction condition, kept constant, gray shaded: variation of concentration.

To find an overall rate expression as a function of the individual reactant concentrations of the entire data set, we consider the variation of the water concentration first (data set number 2) as the adsorption isotherm could be expressed by the multilayer model (in contrast to the adsorption isotherm of isocyanic acid where no adsorption constant could be derived). In the kinetic experiments the water concentration was varied between 0.2 and 10 vol.%, which is equal to a dimensionless pressure p^* between 2×10^{-3} and 1×10^{-1}. According to Eq. (4) the surface concentration of H_2O on the titania is

$$[\mathrm{Ti{-}OH_2}] = [\mathrm{Ti{-}OH_2}]_{\mathrm{Mono}} \frac{K_2 p^*_{\mathrm{H_2O}}}{(1 - p^*_{\mathrm{H_2O}})[1 - (1 - K_2) p^*_{\mathrm{H_2O}}]}, \tag{8}$$

which can be substituted into the rate expression (Eq. (7))

$$r = k_s[\mathrm{Ti{-}NCO}][\mathrm{Ti{-}OH_2}]_{\mathrm{Mono}} \frac{K_2 p^*_{\mathrm{H_2O}}}{(1 - p^*_{\mathrm{H_2O}})[1 - (1 - K_2) p^*_{\mathrm{H_2O}}]}. \tag{9}$$

In order to reduce the number of unknown variables, the rate constant k_s and the isocyanate surface concentration can be combined to one constant k'_s yielding

$$r = k'_s[\mathrm{Ti{-}OH_2}]_{\mathrm{Mono}} \frac{K_2 p^*_{\mathrm{H_2O}}}{(1 - p^*_{\mathrm{H_2O}})[1 - (1 - K_2) p^*_{\mathrm{H_2O}}]}. \tag{10}$$

This equation was used for a non-linear least mean squares (LMS) regression analysis performed by a Levenberg–Marquardt minimization algorithm [37,38] with $[\mathrm{Ti{-}OH_2}]_{\mathrm{Mono}} = 0.722$ mol/l already determined from the thermogravimetric experiment (described in Section 3.2.) to obtain the two variables k'_s and K_2. Fig. 11 shows the fit of the experimental data using $k'_s = 0.037\ \mathrm{s}^{-1}$ and $K_2 = 105$.

In the following steps the simulation of the rate is stepwise expanded including the variation of H_2O, HNCO and NH_3, i.e.

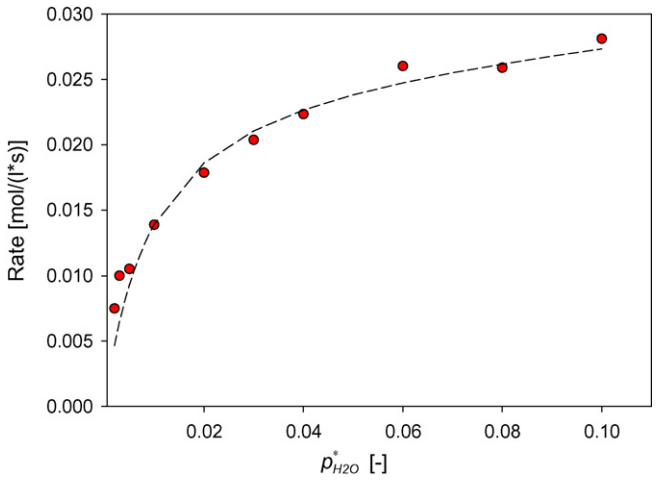

Fig. 11. Preliminary fit for data set number 2, (●) experimental data, (- -) calculated rate.

the whole experimental data at the end (data sets 1–6). In earlier kinetic studies, a decrease in hydrolysis activity in presence of NH_3 was observed which was ascribed to a product inhibition effect suppressing adsorption of HNCO [27]. Therefore, a competitive sorption of HNCO and NH_3 is assumed, and the surface concentration of isocyanate species can be described by:

$$[\mathrm{Ti{-}NCO}] = [\mathrm{Ti{-}NCO}]_{\mathrm{Mono}} \frac{K_1 p^*_{\mathrm{HNCO}}}{1 + K_1 p^*_{\mathrm{HNCO}} + K_3 p^*_{\mathrm{NH_3}}}. \quad (11)$$

By substitution of Eq. (11)) into the rate Eq. (9) the extended rate expression can be obtained

$$r = k_s [\mathrm{Ti{-}NCO}]_{\mathrm{Mono}} \frac{K_1 p^*_{\mathrm{HNCO}}}{1 + K_1 p^*_{\mathrm{HNCO}} + K_3 p^*_{\mathrm{NH_3}}} [\mathrm{Ti} - \mathrm{OH_2}]_{\mathrm{Mono}} \times \frac{K_2 p^*_{\mathrm{H_2O}}}{(1 - p^*_{\mathrm{H_2O}})[1 - (1 - K_2) p^*_{\mathrm{H_2O}}]} \quad (12)$$

or, when combining $k_s[\mathrm{Ti{-}NCO}]_{\mathrm{Mono}}$ into k''_s,

$$r = k''_s \frac{K_1 p^*_{\mathrm{HNCO}}}{1 + K_1 p^*_{\mathrm{HNCO}} + K_3 p^*_{\mathrm{NH_3}}} [\mathrm{Ti} - \mathrm{OH_2}]_{\mathrm{Mono}} \times \frac{K_2 p^*_{\mathrm{H_2O}}}{(1 - p^*_{\mathrm{H_2O}})[1 - (1 - K_2) p^*_{\mathrm{H_2O}}]}. \quad (13)$$

In the next step, the variables k''_s and K_1 were determined using the values for $[\mathrm{Ti{-}OH_2}]_{\mathrm{Mono}}$ and K_2 already calculated. The parameters corresponding to rate expression (13) are summarized in Table 3, and the fit of the model to the variation of the HNCO, H_2O and NH_3 concentration is illustrated in Figs. 12–14.

It can be noted that the rates calculated for the variation of the HNCO concentration are marginally above the experimental data, while for the variation of the H_2O concentration the calculated values for the rate are slightly lower than the experimental data. It was found during carrying out the regression analysis that by varying the starting value of any parameter the two terms for the respective surface concentrations in Eq. (13) could not be addressed independently. Fig. 14 showing the dependence of the overall rate on the NH_3 concentration confirms the inhibiting effect of the hydrolysis product. The wider distribution at the high NH_3 partial pressures is attributed to the higher standard deviation of the measured NH_3 concentration there.

The rate constant k_s can be estimated to be around 6.4×10^{-2} l/(mol s) assuming that $[\mathrm{Ti{-}NCO}]_{\mathrm{Mono}}$ is of the same order of magnitude as $[\mathrm{Ti{-}OH}]_{\mathrm{Mono}}$.

The observed and calculated rates using the model described are compared in the parity plot shown in Fig. 15. The rate expression derived (Eq. (12)) describes the complete data set adequately and systematic deviations were not observed for the model.

Possible deviations from the diagonal are predominantly due to the following reasons: The quantification method for

Table 3
Adsorption constants and combined rate constant (k''_s) estimated on the basis of Eq. (13)

k''_s [s^{-1}]	K_1	K_2	K_3	$[\mathrm{Ti{-}OH_2}]_{\mathrm{Mono}}$ [mol/l]
4.63×10^{-2}	6085	105	3000	0.722

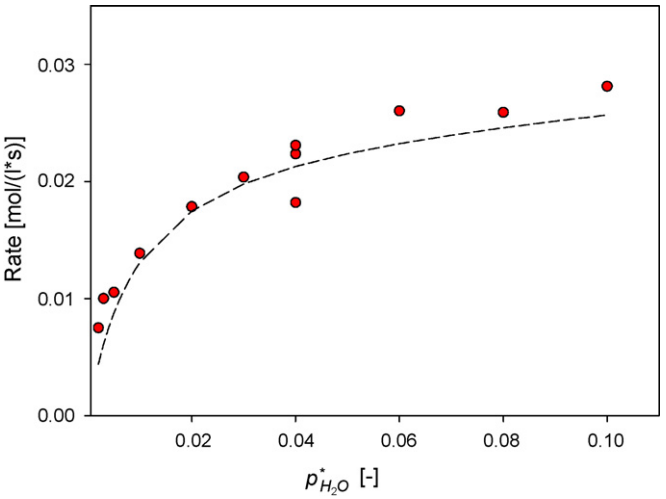

Fig. 13. Correlation between calculated rate (- -) and experimental data (●) in case of variation of H_2O concentration (complete data set considered).

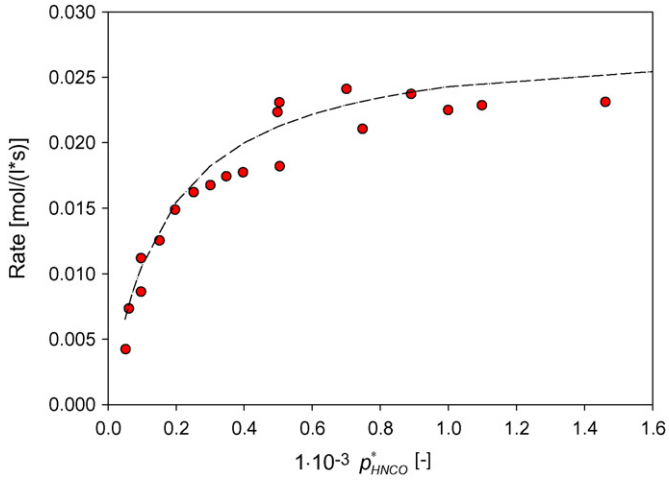

Fig. 12. Correlation between calculated rate (- -) and experimental data (●) in case of variation of HNCO concentration (complete data set considered).

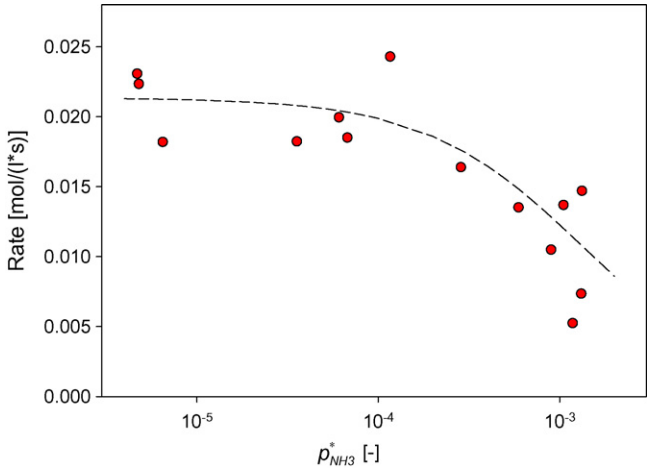

Fig. 14. Correlation between calculated rate (- -) and experimental data (●) in case of variation of NH_3 concentration (complete data set considered).

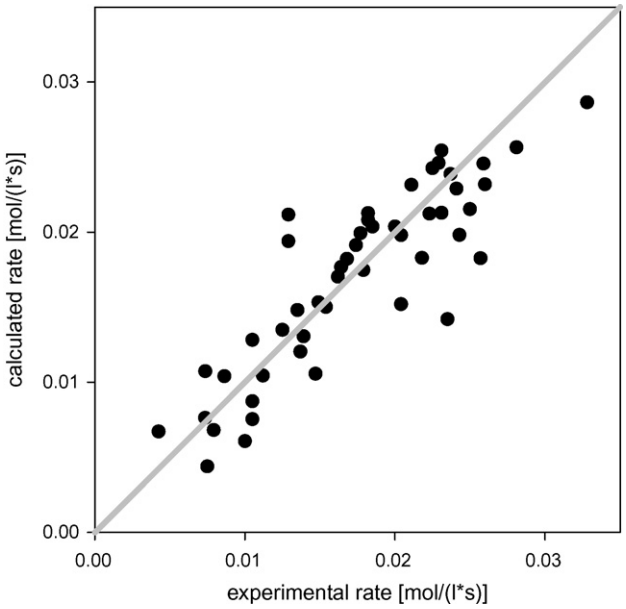

Fig. 15. Parity plot using the complete data set.

determining the gas composition by IR spectroscopy was also used outside the specified concentration ranges of the calibration method. The applied catalysts were prepared as a (single) coated metal sheet of 10 mm length and a thickness of 110 μm. This configuration simulates a two channel monolithic structure with a cell density of 185 cpsi, but the mass of active material exposed to the gas stream was only about 1.75 mg. Although the size of the applied single sheet in the reactor was the same in all experiments (±1% with respect to length), the layer thickness could have varied between the different samples.

4. Conclusions

Sorption isotherms of the reactants of the hydrolysis reaction of isocyanic acid on TiO_2 in anatase modification were determined by means of IR spectroscopy. The sorption isotherm of ammonia follows a Langmuir model while the sorption of water can be described best by the BET isotherm allowing for multilayer adsorption. Isocyanic acid adsorbs dissociatively on Ti^{4+} cations leading to surface coverage of reactive isocyanates Ti–NCO. The adsorption isotherm of isocyanic acid showed a sharp increase of the surface concentration in a narrow pressure range suggesting that a chemical reaction, most likely it is the autocatalytic trimerization of HNCO to cyanuric acid, takes place during sorption. During adsorption of CO_2 on TiO_2 anatase, characteristic carbonate bands were not observed.

The monolayer capacity as well as the equilibrium constants extracted from the sorption isotherms of H_2O and NH_3 were used for a stepwise determination of the other parameters contained in the kinetic model developed for the HNCO hydrolysis reaction. The kinetic model is based on the reaction scheme of elementary steps including the surface reaction of isocyanate with molecularly adsorbed water as the rate-determining step. The sorption and dissociation of HNCO as well as the desorption of NH_3 are significantly faster and do not contribute to the rate determining step. The model and the parameters derived are in good agreement to the experimental data for the rate and the yields.

Acknowledgement

The financial support of the Bayerische Forschungsstiftung under project "Katalytisches Hochleistungssystem zur NO_x-Verminderung für Fahrzeugdieselmotoren-Hochleistungs-GD-KAT" (No. 524/02) is gratefully acknowledged.

References

[1] H.P. Lenz, S. Prüller, Emissionen und Immissionen von Abgaskomponenten, Fortschritt-Berichte VDI, Reihe 12, Nr. 528, VDI-Verlag, Düsseldorf, 2003, p. 16.
[2] P. Forzatti, Appl. Catal. A 222 (2001) 221–236.
[3] H.L. Fang, H.F.M. DaCosta, Appl. Catal. B Environ. 46 (2003) 18–34.
[4] G. Busca, L. Lietti, G. Ramis, F. Berti, Appl. Catal. B Environ. 18 (1998) 1–36.
[5] M. Kleemann, M. Elsener, M. Koebel, A. Wokaun, Ind. Eng. Chem. Res. 39 (2000) 4120–4126.
[6] http://www.acea.be, Position Papers, 30/06/2003.
[7] M. Koebel, M. Elsener, O. Kröcher, C. Schär, R. Röthlisberger, F. Jaussi, M. Mangold, Top. Catal. 30/31 (2004) 43–48.
[8] M. Koebel, E.O. Strutz, Ind. Eng. Chem. Res. 42 (2003) 2093–2100.
[9] E. Jacob, A. Döring, From the SCR catalyst to the controlled diesel catalyst (GD-KAT), Tagungsband VDA Technischer Kongress in Wolfsburg, April 2003, pp. 163–171.
[10] P.M. Schaber, J. Colson, S. Higgins, E. Dietz, D. Thielen, B. Anspach, J. Brauer, Am. Lab. 13 (1999) 13–21.
[11] A.F. Hollemann, Lehrbuch der anorganischen Chemie/Hollemann-Wiberg, 101st ed., de Gruyter, Berlin, New York, 1995.
[12] J.A. Lercher, Z. Zhan, Eur. Patent Appl. 94113599 (1995).
[13] Z. Zhan, Catalytic synthesis and conversion of melamine and its analogues, Ph.D. Thesis, University of Twente, Netherlands, 1995.
[14] G. Mirth, F. Eder, J.A. Lercher, Appl. Spectrosc. 48 (1994) 194–197.
[15] P.L.T. Gabrielsson, Top. Catal. 28 (2004) 177–184.
[16] J.A. Lercher, Z. Phys. Chem. Neue Folge 118 (1979) 209–220.
[17] A.A. Tsyganenko, V.N. Filimonov, Spectrosc. Lett. 5 (1972) 477–487.
[18] G. Ramis, G. Busca, V. Lorenzelli, P. Forzatti, Appl. Catal. 64 (1990) 243–257.
[19] G. Busca, H. Saussey, O. Saur, J.C. Lavalley, V. Lorenzelli, Appl. Catal. 14 (1985) 245–260.
[20] G. Ramis, G. Busca, V. Lorenzelli, J. Chem. Soc. Faraday Trans. I 83 (1987) 1591.
[21] M. Waqif, J. Bachelier, O. Saur, J.C. Lavalley, J. Mol. Catal. 72 (1992) 127–138.
[22] O. Saur, M. Bensitel, A.B. Mohammed Saad, J.C. Lavalley, C.P. Tripp, B.A. Morrow, J. Catal. 99 (1986) 104–110.
[23] H. Knözinger, Adv. Catal. 25 (1976) 209.
[24] T. Bezrodna, G. Puchkovska, V. Shymanovska, J. Baran, H. Ratajczak, J. Mol. Struct. 700 (2004) 175–181.
[25] P.W. Atkins, Physikalische Chemie, third corrected ed., Wiley-VCH, Weinheim, 2001.
[26] C.-T. Liu, W.T. Lindsay Jr., J. Chem. Eng. Data 15 (1970) 510–513.
[27] Ph. Hauck, A. Jentys, J.A. Lercher, Appl. Catal. B Environ. 70 (2007) 91–99.
[28] G. Fischer, J. Geith, T.M. Klapötke, B. Krumm, Z. Naturforsch. 57b (2002) 19–24.
[29] F. Solymosi, T. Bánsági, J. Phys. Chem. 83 (1979) 552–553.
[30] G. Piazzesi, O. Kröcher, M. Elsener, A. Wokaum, Appl. Catal. B Environ. 65 (2006) 55–61.
[31] F. Acke, B. Westerberg, M. Skoglundh, J. Catal. 179 (1998) 528–536.

[32] M.A. Larrubia, G. Ramis, G. Busca, Appl. Catal. B Environ. 30 (2001) 101–110.
[33] A. Schmidt, Monatsh. Chem. 99 (1968) 664–671.
[34] R. Roudit, A. Baiker, F. Bettoni, J. Baldyga, A. Wokaun, AIChE J. 44 (12) (1998) 2731.
[35] P.G. Mass, Oxidative Dehydrierung von Propan über getragenen Chromoxidkatalysatoren, Ph.D. Thesis, Technische Universität München, 1998.
[36] T. Homann, T. Bredow, K. Jug, Surf. Sci. 555 (2004) 135–144.
[37] K. Levenberg, Q. Appl. Math. 11 (1944) 164–168.
[38] D.W. Marquardt, J. Soc. Ind. Appl. Math. 11 (1963) 431–441.